JACS
JOURNAL OF THE AMERICAN CHEMICAL SOCIETY
Article
pubs.acs.org/JACS

The Electronic Nature of Terminal Oxo Ligands in Transition-Metal Complexes: Ambiphilic Reactivity of Oxorhenium Species

Jessica L. Smeltz,† Cassandra P. Lilly,† Paul D. Boyle, and Elon A. Ison*

Department of Chemistry, North Carolina State University, 2620 Yarbrough Drive, Raleigh, North Carolina 27695-8204, United States

Supporting Information

ABSTRACT: The synthesis of the Lewis acid−base adducts of $B(C_6F_5)_3$ and BF_3 with [DAAmRe(O)(X)] DAAm = *N*,*N*-bis(2-arylaminoethyl)methylamine; aryl = C_6F_5 (X = Me, **1**, $COCH_3$, **2**, Cl, **3**) as well as their diamidopyridine (DAP) (DAP=(2,6-bis((mesitylamino)methyl)pyridine) analogues, [DAPRe(O)(X)] (X = Me, **4**, Cl, **5**, I, **6**, and $COCH_3$, **7**), are described. In these complexes the terminal oxo ligands act as nucleophiles. In addition we also show that stoichiometric reactions between **3** and triarylphosphine (PAr_3) result in the formation of triarylphosphine oxide ($OPAr_3$). The electronic dependence of this reaction was studied by comparing the rates of oxygen atom transfer for various para-substituted triaryl phosphines in the presence of CO. From these experiments a reaction constant $\rho = -0.29$ was obtained from the Hammett plot. This suggests that the oxygen atom transfer reaction is consistent with nucleophilic attack of phosphorus on an electrophilic metal oxo. To the best of our knowledge, these are the first examples of mono-oxo d^2 metal complexes in which the oxo ligand exhibits ambiphilic reactivity.

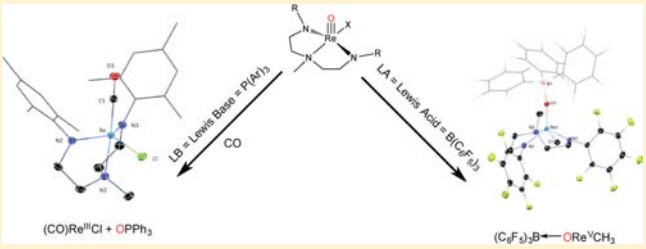

INTRODUCTION

Oxo metal complexes are pervasive and are proposed as intermediates in many important catalytic reactions. For example, iron(IV) oxo complexes are believed to be intermediates in oxidation reactions catalyzed by heme-containing enzymes.[1] Also, oxidations catalyzed by enzymes that contain the molybdopterin prosthetic group are believed to be composed of oxo molybdenum complexes and are responsible for catalytic oxygen atom transfer reactions.[2] The active site of the oxygen evolving complex (OEC), in photosystem II (PSII), consists of a proposed Mn intermediate that utilizes a terminal oxo ligand for water oxidation.[3] In synthetic analogues, such as the ruthenium "blue dimer" catalyst, a terminal Ru oxo is utilized.[4] Since in many of these catalysts, reactions at the terminal oxo are critical, it is important to understand the electronic nature of the oxo ligand in order to rationally design new catalysts or to understand catalytic systems such as PSII.

Gray and others have provided valuable insight into the nature of metal oxo bonds.[5] They have shown that the oxo ligand in mono-oxo complexes with d^0−d^2 electron configurations in a tetragonal environment, are considered to be electrophilic because of π bonding between the oxygen lone pairs and the d_{xz} and d_{yz} orbitals on the metal center (Figure 1). In d^2 complexes, the two d-electrons occupy the d_{xy} nonbonding orbital and the bond order for the metal oxo bond is 3. In d^4 complexes, the addition of extra electrons results in a decrease in bond order as electrons occupy orbitals that are π antibonding. The oxo ligand in these cases is considered to be nucleophilic.

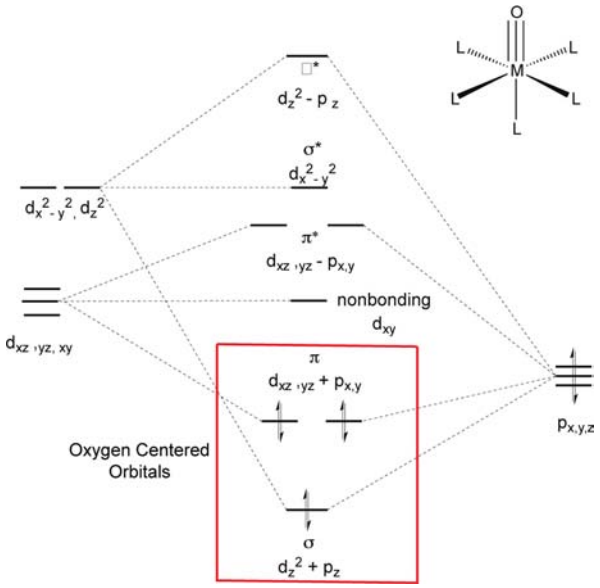

Figure 1. Bonding in d^0 octahedral transition-metal oxo complexes.

The electrophilic nature of terminal oxo ligands is often used to explain reactivity. For example, catalytic asymmetric epoxidation is believed to proceed by the nucleophilic attack of an olefinic substrate on an electrophilic terminal oxo ligand.[6]

Received: February 10, 2013
Published: May 31, 2013

dx.doi.org/10.1021/ja401390v | J. Am. Chem. Soc. 2013, 135, 9433−9441

Catalytic oxygen atom-transfer reactions to phosphines and sulfides also proceed via electrophilic oxo intermediates.[7]

The orbital energy level diagram depicted in Figure 1 can be perturbed however by the judicious choice of ancillary ligands.[8] For example, the electronic character of the terminal oxo may be altered by incorporating ligands that can change the energy of the σ (d_z^2 + p_z) and π ($d_{yz,xz}$ + $p_{x,y}$) orbitals. Thus, the incorporation of electron donating ligands may raise the energy of these orbitals and consequently alter the electrophilicity of the terminal oxo.

In this paper, the synthesis of the Lewis acid−base adducts of $B(C_6F_5)_3$ with [DAAmRe(O)(X)] DAAm = *N*,*N*-bis(2-arylaminoethyl)methylamine; aryl = C_6F_5 (X = Me, **1**, $COCH_3$, **2**, Cl, **3**) as well as their diamidopyridine (DAP) (DAP = (2,6-bis((mesitylamino)methyl)pyridine) analogues, [DAPRe(O)(X)] (X = Me, **4**, Cl, **5**, I, **6**, and $COCH_3$, **7**) are described.[9] In these complexes the terminal oxo ligands act as nucleophiles. In addition we also show that stoichiometric reactions between **3b** (aryl = Mes) and triarylphosphine (PAr_3) in the presence of CO result in the formation of triarylphosphine oxide ($OPAr_3$) and the Re(III) complex, [DAAmRe(CO)Cl], **21**. The electronic dependence of this reaction was studied by comparing the rates of oxygen atom transfer for various para-substituted triaryl phosphines. These data are consistent with nucleophilic attack of the triaryl phosphine substrate on the terminal oxo ligand, i.e., the terminal oxo ligand in this case, acts as an electrophile. To the best of our knowledge, these are the first examples of mono−oxo d^2 metal complexes in which the oxo ligand exhibits ambiphilic reactivity.

RESULTS AND DISCUSSION

Nucleophilic Reactivity of the Rhenium Oxos. Complexes **1** and **3** were prepared as previously reported.[9] The slow diffusion of pentane overnight into a concentrated dichloromethane solution of these complexes mixed with tris(pentafluorophenyl)boron ($B(C_6F_5)_3$) at room temperature resulted in the isolation of the complexes **8** and **9**, where the $B(C_6F_5)_3$ reagent forms a Lewis acid−base adduct with the terminal oxo ligand (Scheme 1).

Scheme 1

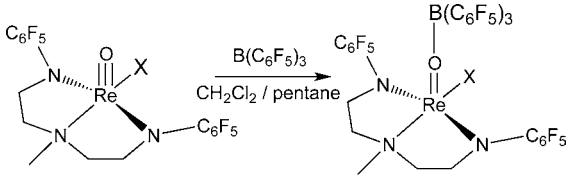

X = Me, **1**; Cl, **3** X = Me, **8**; Cl, **9**

X-ray crystal structures of each of these complexes were obtained. Complexes **8** and **9** are geometrically similar to their corresponding starting complexes. A distorted square pyramidal structure around the rhenium atom with the oxo−boron (O1−B1) ligand in the apical position is observed in **8** (Figure 2). The Re1−O1 bond length in **8** is elongated by 0.07 Å, compared to the analogous bond in **1**. This lengthening of the metal-oxo bond is the same magnitude observed in other metal−oxo−boron systems.[10] The Re1−O1−B1 bond angle is approximately 170°. Similar M−O−$B(C_6F_5)_3$ bond angles have been reported.

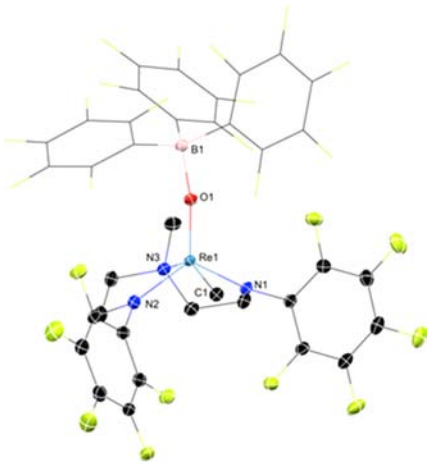

Figure 2. Thermal ellipsoid plot of complex **8**. Thermal ellipsoids are at 50%. H atoms have been omitted for clarity. In addition, the C_6F_5 fragment on $B(C_6F_5)_3$ has been depicted in wireframe for clarity. Selected bond lengths (Å) and angles (°): Re1−O1, 1.7514(13); Re1−C1, 2.1240(19); Re1−N1, 1.9437(15); Re1−N2, 2.1630(17); O1−B1, 1.559(2); N1−Re1−N2, 78.75(6); N1−Re1−N3, 117.53(7); N1−Re1−C1, 85.51(7); N2−Re1−C1, 147.63(6); Re1−O1−B1, 169.81(12); O1−Re1−C1, 101.68(7); O1−Re1−N1, 119.24(6); O1−Re1−N2, 110.70(6).

The stability of the DAAm complexes in solution is very poor, as decomposition is rapidly observed in the presence of trace amounts of water and in halogenated solvents. This complicates spectroscopic characterization of the DAAm complexes, and as a result, the DAP analogues were similarly prepared, and their increased stability allowed for spectroscopic characterization.

Complexes **4**−**6** were prepared as previously published.[9a,b] The addition of $B(C_6F_5)_3$ to a solution that contained **4**−**6** dissolved in a minimal amount of dichloromethane, followed by the slow diffusion of pentane overnight resulted in the isolation of the Lewis acid−base adducts **10**−**12** (Scheme 2).

Scheme 2

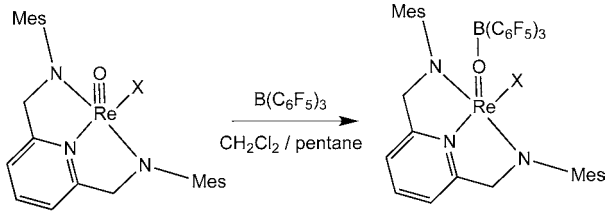

X = Me, **4**; Cl, **5**; I, **6** X = Me, **10**; Cl, **11**; I, **12**

X-ray crystal structures of **10**−**12** were obtained. The geometry at rhenium in **10** is best described as a distorted square pyramid (Figure 3) with the oxo ligand (O1) in the apical position. Complexes **11** and **12** are isostructural complexes with the chloride ligand replaced by an iodide. The structural characteristics of **10**−**12** are similar to the starting complexes **4**−**6**. Similar to the DAAm complexes, the Re1−O1 bond length in **10** is elongated by 0.07 Å compared to the rhenium oxo bond in complexes **4**. In the ^{1}H NMR spectrum for **10** a downfield shift (compared to **4**) of the methylene protons from 5.63 and 5.42 ppm to 6.12 and 5.61

dx.doi.org/10.1021/ja401390v | J. Am. Chem. Soc. 2013, 135, 9433−9441

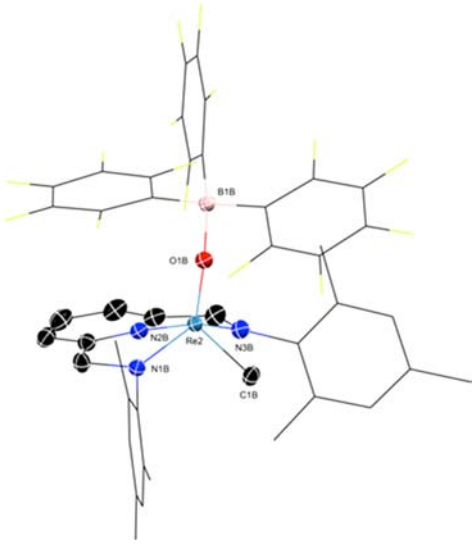

Figure 3. Thermal ellipsoid plot of complex **10**. Thermal ellipsoids are at 50%. H atoms have been omitted for clarity. In addition, the C_6F_5 fragment on $B(C_6F_5)_3$ and the Mes fragment on the DAP ligand have been depicted in wireframe for clarity. Selected bond lengths (Å) and angles (°): Re2−O1B, 1.7557(19); Re2−N1B, 1.951(2); Re2−N2B, 2.037(2); Re2-ClB, 2.101(3); O1B−B1B, 1.526(3); O1B−Re2−N3B, 110.94(9); O1B−Re2−N1B, 113.14(9); N3B−Re2−N1B, 135.40(9); O1B−Re2−N2B, 118.88(9); N3B−Re2−N2B, 76.62(9); N1B−Re2−N2B, 76.67(9); O1B−Re2−C1B, 104.46(10); N3B−Re2−C1B, 88.34(10); N1B−Re2−C1B, 87.23(6); N2B−Re2−C1B, 136.66(10); B1B−O1B−Re2, 175.38(18).

ppm was observed. In addition, the methyl protons were observed at 3.46 ppm compared to 1.76 ppm in **4**.

Isolation of the DAAm and DAP Lewis acid−base adducts **8**, **9** and **10**−**12** are indicative of the nucleophilic reactivity of the terminal oxo in these complexes. Similar reactivity was observed for the reaction of complex **5** with MeMgBr to produce **4** (Scheme 3). When the progress of this reaction was followed

Scheme 3

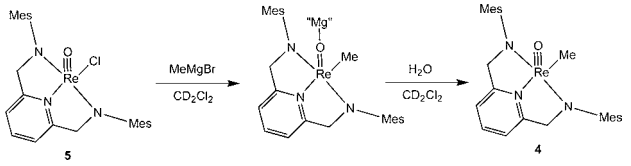

by ^{1}H NMR spectroscopy, a shift in the methylene protons in **5** to 6.05 and 5.54 ppm was observed. These chemical shifts are similar to chemical shifts observed in the formation of the Lewis acid−base adducts (**10**−**12**) described above. Addition of water to this reaction mixture led to the formation of **4**.

Nucleophilicity of the Rhenium Oxo in a Complex Bearing Two Nucleophilic Sites. *Reactions with $B(C_6F_5)_3$.* The addition of $B(C_6F_5)_3$ to complex **2** and the DAP derivative **7** was of interest, as these complexes bear two nucleophilic sites: (1) the terminal oxo and (2) the acyl oxygen. The addition of $B(C_6F_5)_3$ to **2** and **7** could result in the binding of the Lewis acid at the acyl oxygen; however, binding at the terminal oxo ligand was observed and the Lewis acid−base complexes **13** and **14** resulted (Scheme 4).

X-ray quality crystals of **13** and **14** were obtained and verified the addition of the Lewis acid to the terminal oxo ligand

Scheme 4

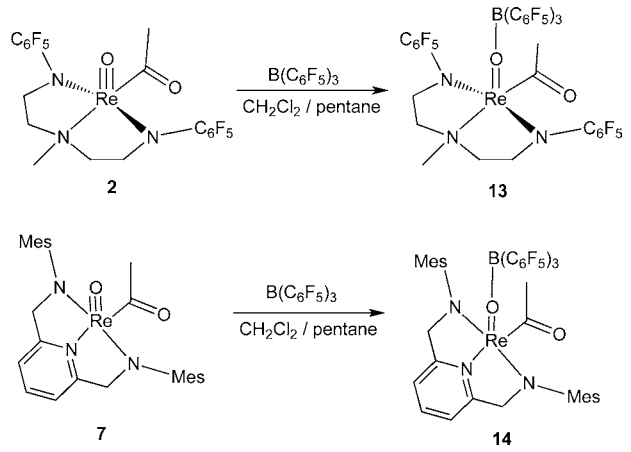

(Figure 4 and 5). The geometry around the rhenium atom in **13** and **14** is best described as distorted square pyramidal with

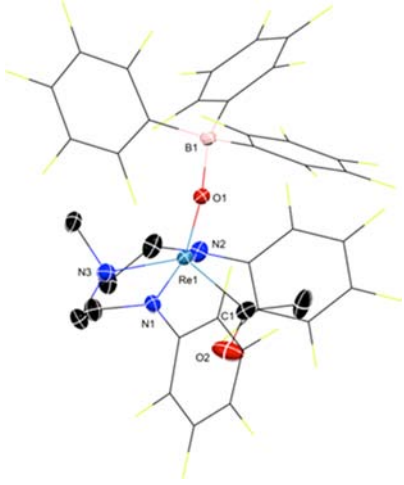

Figure 4. Thermal ellipsoid plot of complex **13**. Thermal ellipsoids are at 50%. H atoms have been omitted for clarity. In addition, the C_6F_5 fragment on $B(C_6F_5)_3$ and the DAAm ligand have been depicted in wireframe for clarity. Selected bond lengths (Å) and angles (°): Re1−O1, 1.7479(19); Re1−C1, 2.004(3); Re1−N1, 1.973(2); Re1−N2, 2.142(3); O1−B1, 1.581(4); C1−O2, 1.213(4); N1−Re1−N2, 78.59(10); N1−Re1−N3, 144.18(10); N1−Re1−C1, 85.90(11); N2−Re1−C1, 125.94(11); Re1−O1−B1, 171.52(18); O1−Re1−C1, 112.33(11); O1−Re1−N1, 108.36(10); O1−Re1−N2, 121.72(9).

the oxo−boron ligand (O1−B1) in the apical position. These are only the second and third examples of a metal−oxo−boron adduct that contains an acyl ligand.[10d] However, in the previously reported complex, the acyl ligand is bound in an η^2 fashion. The rhenium oxo bonds in **13** and **14** are elongated by 0.06 and 0.07 Å, respectively. This elongation is similar to that observed in the other Lewis acid−base adducts described above.

In addition, the acyl (C═O) stretch for **13** (1649 cm^{-1}) is shifted to higher frequency compared to **2** (1582 cm^{-1}). The shift to higher wavenumbers indicates the C═O bond in **13** is strengthened relative to **2** as a result of decreased π-back-donation from rhenium to the acyl carbon, presumably because the metal center in **13** is more electron deficient. The change in frequency indicates a significant contribution from the carbene-

dx.doi.org/10.1021/ja401390v | *J. Am. Chem. Soc.* 2013, 135, 9433−9441

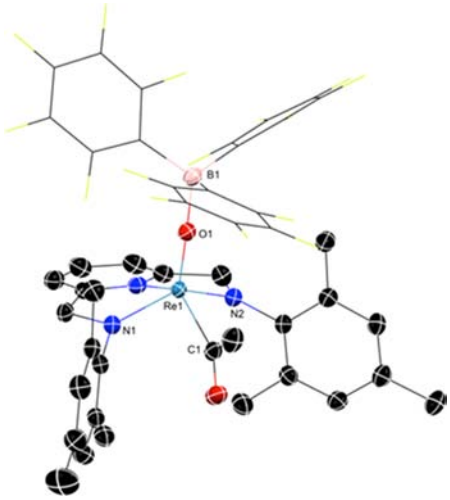

Figure 5. Thermal ellipsoid plot of complex **14**. Thermal ellipsoids are at 50%. H atoms have been omitted for clarity. In addition, the C_6F_5 fragment on $B(C_6F_5)_3$ has been depicted in wireframe for clarity. Selected bond lengths (Å) and angles (°): Re1−O1, 1.7725(12); Re1−N1, 1.9612(16); Re1−N2, 2.0342(16); Re1−C1, 2.0380(19); O1−B1, 1.529(2); O1−Re1−N3, 110.64(6); O1−Re1−N1, 113.01(6); N3−Re1−N1, 135.90(6); O1−Re1−N2, 135.90(6); N3−Re1−N2, 76.74(6); N1−Re1−N2, 76.74(6); O1−Re1−C1, 107.84(7); N3−Re1−C1, 85.09(7); N1−Re1−C1, 87.51(7); N2−Re1−C1, 132.44(7); Re1−O1−B1, 169.48(12).

like resonance structure B for **2**, whereas **13** is more acyl-like and is consistent with resonance structure A (Scheme 5).

Scheme 5

In the ^{1}H NMR spectrum for **13** two isomers are observed in which the acyl oxygen is oriented syn and anti with respect to the oxo-boron ligand. Two isomers of the parent complex **2** were also observed.[11] Crystallization of **13** allows for isolation of only one isomer.

Reactions with BF_3·OEt_2. The reaction of **2** with BF_3 was also investigated. BF_3·OEt_2 was added to **2** in a concentrated methylene chloride solution. Slow diffusion of pentane into the reaction mixture overnight led to the formation of X-ray quality crystals that confirm the binding of BF_3 at the acyl oxygen to yield **15** (Scheme 6, Figure 6). The geometry around the rhenium atom in **15** is best described as distorted square pyramidal with the oxo ligand (O1) in the apical position. As shown in Figure 7, BF_3 is oriented anti with respect to the acyl methyl. A weak Lewis acid−base interaction between one of the fluorine atoms from BF_3 and the rhenium atom is observed in the crystal structure, where the Re1−F1 distance is 2.65 Å, and the B1−F1 bond length is slightly longer (1.403 Å) than the B1−F2 (1.361 Å) or B1−F3 (1.379 Å). The Re1−C1 bond length in **15** is slightly shorter (0.018 Å) than the Re−C_{acyl} bond length in **2**. This suggests that there is significant multiple bonding character in the metal carbon bond. Also, the ^{13}C NMR chemical shift for the acyl carbon in **15** is 299 ppm compared to 265 ppm in **2**, this is consistent with resonance structure B (Scheme 5). Similarly, the slow diffusion of pentane overnight into a reaction mixture that contained **7** and

Scheme 6

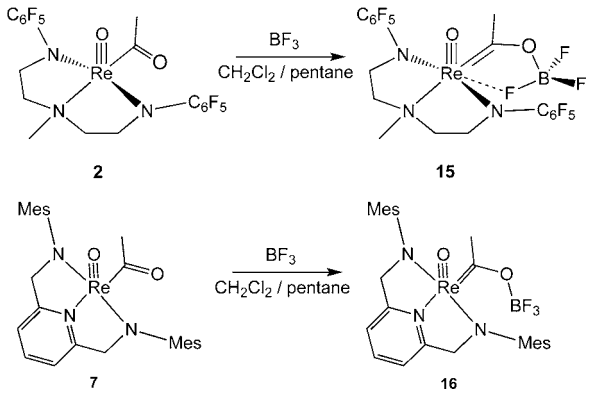

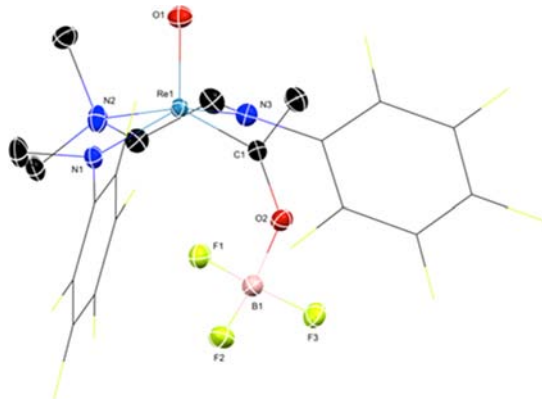

Figure 6. Thermal ellipsoid plot of complex **15**. Thermal ellipsoids are at 50%. H atoms have been omitted for clarity. In addition, the C_6F_5 fragment on the DAAm ligand has been depicted in wireframe for clarity. Selected bond lengths (Å) and angles (°): Re1−O1, 1.6766(13); Re1−N1, 1.9893(15); Re1−N2, 2.1805(17); Re1−C1, 2.0074(18); C1−O2, 1.286(2); O2−B1, 1.516(2); B1−F1, 1.403(2); B1−F2, 1.361(2); B1−F3, 1.379(2); O1−Re1−N1, 106.67(7); O1−Re1−N2, 107.83(6); O1−Re1−C1, 99.92(7); N1−Re1−N2, 78.26(6); N1−Re1−N3, 143.58(6); N1−Re1−C1, 93.92(7); N2−Re1−C1, 152.25(6); Re1−C1−O2, 128.48(12); C1−O2−B1, 124.66(14).

BF_3·OEt_2 led to the formation of **16** (Scheme 6). The ^{13}C NMR chemical shift in **16** is observed at 299 ppm compared to 259 ppm in **7**.

DFT Calculations. The electronic nature of the oxo ligands in many of the complexes described above was investigated by DFT calculations.[12] All calculations were performed with the 6-31G(d, p) basis set[13] on the B, C, F, H, N, and O atoms and the SDD pseudopotential and basis set augmented with an *f* polarization function on the Re atom.[14] Solvation energies were calculated with dichloromethane as the solvent by applying the SMD[15] solvation model, as implemented in Gaussian 09,[16] to structures optimized in the gas phase. All energies are reported in kcal/mol with the solvation energies reported without parentheses and gas-phase energies in parentheses.

We were particularly interested in the reaction of acyl complexes **2** and **7** with Lewis acids because, as stated above, these complexes contain two nucleophilic sites. In order to determine whether $B(C_6F_5)_3$ and BF_3 add preferentially to the terminal oxo or the acyl oxygen because of electronic or steric factors, calculations were performed to compare the energetics for binding at both sites.

dx.doi.org/10.1021/ja401390v | J. Am. Chem. Soc. 2013, 135, 9433−9441

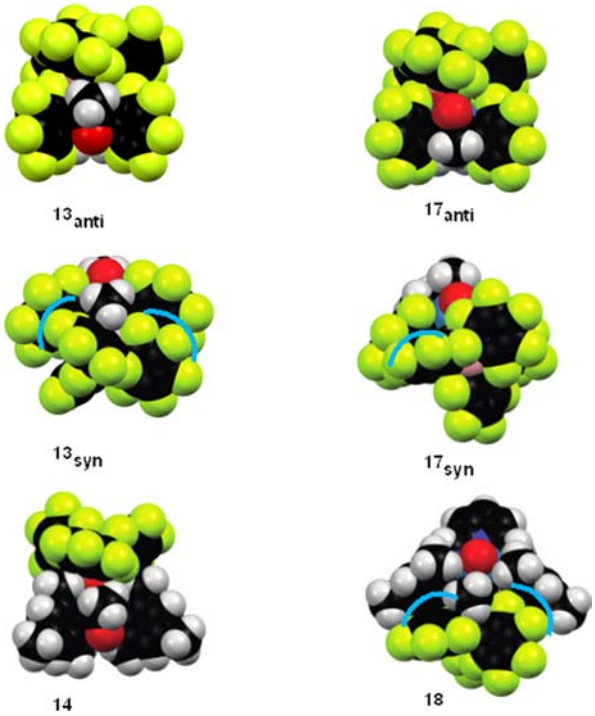

Figure 7. Space filled diagrams for the reaction of $B(C_6F_5)_3$ at the terminal oxo in $\mathbf{13}_{anti}$ (top left) $\mathbf{13}_{syn}$ (middle left), and **14** (bottom left), and the reaction at the acyl oxygen in $\mathbf{17}_{anti}$ (top right), $\mathbf{17}_{syn}$ (middle right), and **18** (bottom right).

Complex **2** exists as two isomers, $\mathbf{2}_{syn}$ and $\mathbf{2}_{anti}$, where the acyl oxygen is oriented on the same side as the terminal oxo and 180° from the terminal oxo, respectively.[9c,e] As a result, the addition of $B(C_6F_5)_3$ and BF_3 to the terminal oxo and the acyl oxygen in both isomers was investigated. In addition, the reaction of $B(C_6F_5)_3$ and BF_3 with **7** was examined.

The addition of $B(C_6F_5)_3$ to the terminal oxo in **2** results in **13**. Complex $\mathbf{13}_{anti}$ (acyl oriented anti to the terminal oxo) was found to be 2.4 kcal/mol more stable on the free energy surface than $\mathbf{13}_{syn}$ (acyl oriented syn to the terminal oxo), and the free energy of activation for conversion between the two isomers is 21.6 kcal/mol.

Similarly, the addition of $B(C_6F_5)_3$ to the terminal oxo in **7** results in **14**. Importantly complexes $\mathbf{13}_{anti}$, $\mathbf{13}_{syn}$, and **14**, were found to be 3.5, 2.2, and 11.1 kcal/mol more stable on the free energy surface than complexes $\mathbf{17}_{anti}$, $\mathbf{17}_{syn}$, and **18**, where the Lewis acid is bound to the acyl oxygen (Schemes 7 and 8).

This is again consistent with experimental data as $\mathbf{13}_{anti}$ and **14** were the only products isolated from the reaction of **2** and **4** with $B(C_6F_5)_3$, respectively. Space filled models were examined in order to compare the steric interactions in the DAAm complexes $\mathbf{13}_{anti}$, $\mathbf{13}_{syn}$, $\mathbf{17}_{anti}$, and $\mathbf{17}_{syn}$ and the DAP complexes **14** and **18** (Figure 7). As depicted in this figure, the likely reason for the increased stability associated with binding at the terminal oxo is the steric congestion associated with adding the bulky Lewis acid, $B(C_6F_5)_3$, to the acyl oxygen.

DFT calculations were also used to examine the energetics of binding the less bulky Lewis acid trifluoroboron, BF_3. To begin, binding of BF_3 at the terminal oxo for the two isomers of **2** was investigated. Binding at the terminal oxo of $\mathbf{2}_{anti}$ to yield $\mathbf{19}_{anti}$ was 5.7 kcal/mol more stable than binding at the terminal oxo for the syn isomer to yield $\mathbf{19}_{syn}$. Therefore, the energetics for binding at the terminal oxo in $\mathbf{19}_{anti}$ was compared to binding at the acyl ligand.

Scheme 7

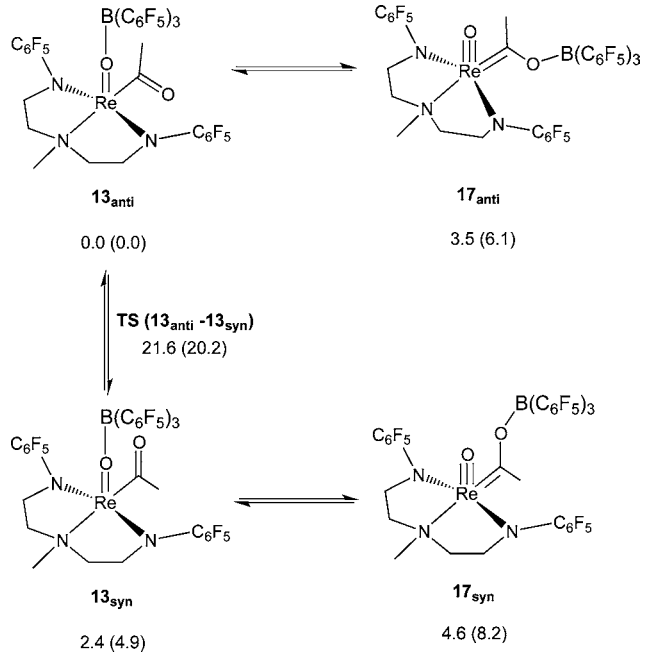

Scheme 8

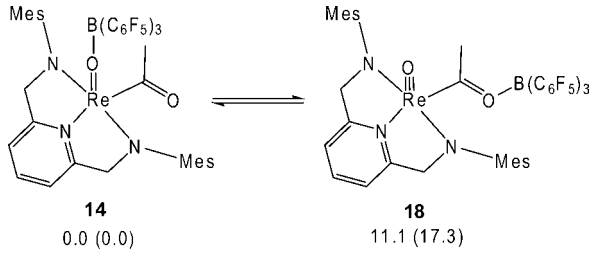

Binding of BF_3 to the acyl oxygen in $\mathbf{2}_{anti}$ was found to be 8.3 kcal/mol more stable than binding to the acyl oxygen in $\mathbf{2}_{syn}$. When BF_3 was bound to the acyl ligand in $\mathbf{2}_{anti}$ two isomers of **15** were found. In one isomer the BF_3 moiety is oriented on the same side of the CH_3 fragment, $\mathbf{15}_{anti}$, while in the other isomer the BF_3 moiety is oriented ~180° from the CH_3 fragment, $\mathbf{15}_{anti'}$, (Scheme 9).

On the free energy surface, $\mathbf{15}_{anti'}$ was found to be 3.4 kcal/mol more stable than $\mathbf{15}_{anti}$ in the gas phase. The structure of $\mathbf{15}_{anti'}$ is similar to the structure of **15** obtained from X-ray crystallography (vide supra). However, when solvation effects were considered $\mathbf{15}_{anti}$ was found to be 4.8 kcal/mol more stable than $\mathbf{15}_{anti'}$. The free energy of activation for the conversion of $\mathbf{15}_{anti'}$ to $\mathbf{15}_{anti}$ in solution is 15.9 kcal/mol. The size of this barrier suggests that in solution, the two isomers may rapidly interconvert on the NMR time scale.

Importantly, binding at the acyl oxygen in $\mathbf{2}_{anti}$ to yield $\mathbf{15}_{anti}$ was found to be 5.0 kcal/mol more stable than binding at the terminal oxo to yield $\mathbf{19}_{anti}$ (Scheme 9). This infers that when steric factors for binding of the Lewis acid are eliminated, the most nucleophilic oxo in the complex is the acyl-oxygen and not the terminal oxo. However, it is noteworthy that the terminal oxo is still sufficiently nucleophilic, even in **2a**, to activate Lewis acids.

dx.doi.org/10.1021/ja401390v | J. Am. Chem. Soc. 2013, 135, 9433−9441

Scheme 9

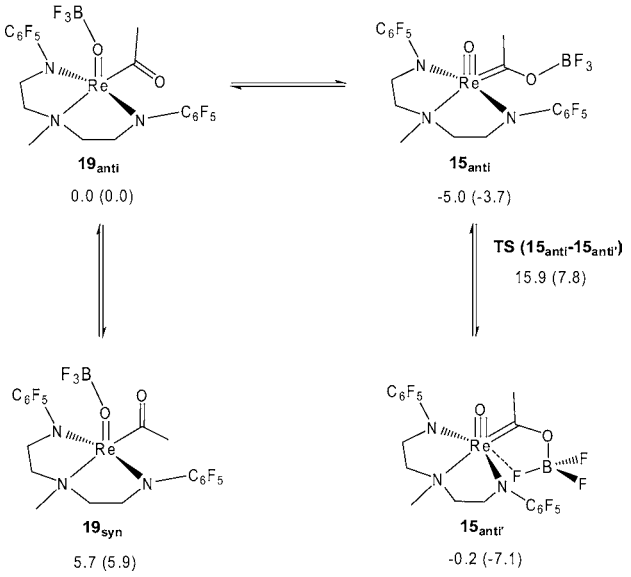

This is further exemplified when the energetics for the binding of BF_3 to **7** were examined. Binding of BF_3 at the terminal oxo to yield **20** was found to be only 0.7 kcal/mol more endergonic than binding at the acyl oxygen to yield **16** (Scheme 10). These results suggest that for this complex the nucleophilic character at the two oxo sites is similar.

Scheme 10

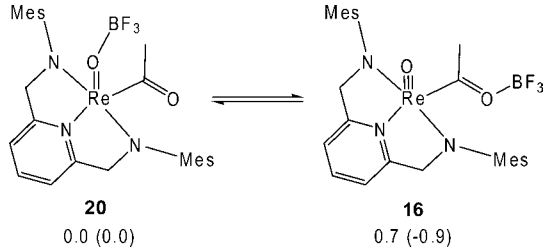

To summarize, both the terminal oxo and the acyl exhibit nucleophilic characteristics when reacted with Lewis acids. When the bulky $B(C_6F_5)_3$ is utilized as the Lewis acid, preferential binding at the terminal oxo is observed. However, when the less sterically demanding Lewis acid BF_3 is employed, binding at the acyl oxygen is preferred with the DAAm complexes. For the DAP complexes the terminal oxo and the acyl oxygen exhibit comparable nucleophilicity, as binding at the terminal oxo is only 0.7 kcal/mol more endergonic than binding at the acyl oxygen. These results suggest that with the appropriate set of ancillary ligands high-valent metal complexes that feature terminal oxo ligands can be tuned to react as nucleophiles.

Electrophilic Reactivity of Rhenium Oxos. In the preceding sections, we have shown numerous examples of high-valent complexes that incorporate terminal mono-oxo ligands and act as nucleophiles. However as noted in Figure 1, these complexes traditionally exhibit electrophilic reactivity at the terminal oxo because of the strong π bonding from the oxygen lone pairs to the transition metal. In fact, electrophilic reactivity has been used to explain the behavior of many high-valent metal oxo complexes that are utilized as catalysts. For example, the mechanism for enantioselective olefin epoxidation catalyzed by (salen)Mn is proposed to proceed by the nucleophilic attack of the olefinic substrate on a oxomanganese intermediate.[6] In addition oxygen atom transfer to substrates catalyzed by oxorhenium(V) catalysts are believed to proceed by the nucleophilic attack of substrates on dioxorhenium(VII) intermediates.

Hammett correlations have frequently been used to probe the electrophilicity of oxo intermediates in many catalytic oxygen atom transfer reactions. For example, Espenson and co-workers utilized MeReO(mtp)PPh_3, where $mtpH_2$ = 2-(mercaptomethyl)thiophenol as a catalyst for the oxygen atom transfer reaction of 4-picoline-N-oxide to $(Ar)_3P$. The mechanism for this reaction is complex, however for the key OAT elementary step, a reaction constant, $\rho = -0.70$, was observed.[7j] This negative reaction constant was interpreted by the authors as resulting from the phosphine substrate acting as a nucleophile and attacking the oxo group of a dioxorhenium-(VII) intermediate. Similarly, our group has recently shown that the complexes [DAAmRe(O)(X)] and [(DAP)Re(O)(X)] (X = Me, Cl, I) are catalysts for the OAT reaction from pyridine N-oxide to triarylphosphines. Through competition experiments with [DAAmRe(O)(Cl)] (aryl = C_6F_5) as the catalyst, an analysis of the kinetic effects on the reaction of pyridine N-oxide with para-substituted triaryl phosphines, resulted in a reaction constant of $\rho = -0.30$.[7l] These data inferred that the reaction proceeds via nucleophilic attack by phosphine on the oxo ligand in a purported Re(VII) dioxo intermediate.

We were interested in examining the nucleophilic attack of phosphine on the terminal oxo in the Re(V) complex **3** according to Scheme 11. The reaction of **3b** (aryl = 2,4,6-

Scheme 11

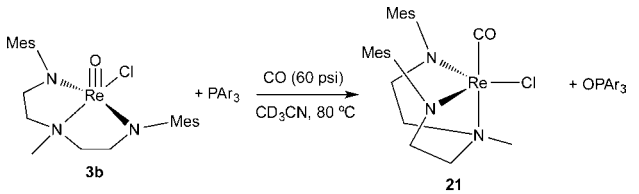

trimethylphosphine (Mes)) with triphenylphosphine in the presence of CO resulted in the reduced rhenium complex [DAAmRe(CO)(Cl)] (aryl = Mes) (**21**). The reaction appeared to be quantitative (within experimental error) by ^1H NMR spectroscopy (versus a ferrocene internal standard) and ^{31}P NMR spectroscopy (1 equiv of $OPPh_3$ was detected). However, because of the poor stability of **21** in solution, the complex could only be isolated in modest yields. X-ray quality crystals of **21** could be obtained by the slow diffusion of pentane into a concentrated methylene chloride solution of the reaction mixture (Figure 8). Compound **21** adopts a distorted trigonal bipyramidal geometry with the CO ligand and the amine nitrogen in the apical positions.

The kinetics for the formation of **21** was monitored by ^1H NMR spectroscopy by observing the reaction of **3b** with excess PPh_3 in the presence of CO (60 psi). As shown in Figure 9, the formation of **21** proceeds exponentially in near quantitative yield. The reaction exhibits first-order dependencies on [PPh_3] and [Re] and saturation kinetics on *p*CO. These data are consistent with the mechanism depicted in Scheme 12, which

dx.doi.org/10.1021/ja401390v | J. Am. Chem. Soc. 2013, 135, 9433−9441

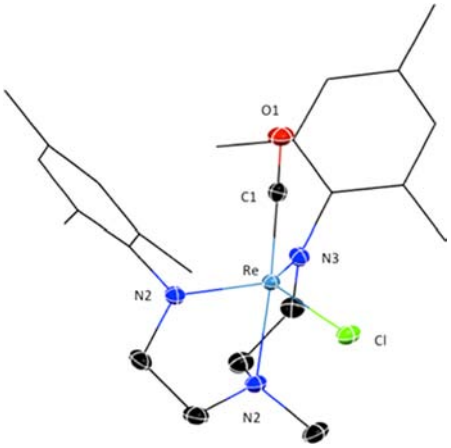

Figure 8. Thermal ellipsoid plot of **21**. Thermal ellipsoids are at 50%. Hydrogen atoms are omitted for clarity. Selected bond lengths (Å) and angles (deg). Re1−C1, 1.8706(15); C1−O1, 1.1651(18); Re1−N1, 1.9115(14); Re1−N2, 2.2287(12); Re1−Cl1, 2.3295(4); C1−Re1−N1, 95.95(7); C1−Re1−N2, 173.91(6); C1−Re1−Cl1, 96.17(4); N1−Re1−Cl1, 114.81(5); N1−Re1−N3, 120.59(6); N1−Re1−N2, 81.81(6); Cl1−Re1−N2, 89.91(4).

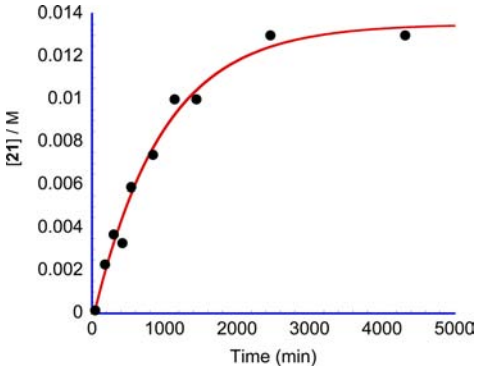

Figure 9. Time course for the reaction of **3b** with PPh_3 and CO (60 psi). Reaction conditions: [Re] = 0.014 M; [PPh_3] = 0.14 M; *p*CO = 60 psi. Reactions were performed in CD_3CN at 80 °C in 5 mL storage tubes for a fixed period of time. Each point represents a different time point. The [**21**] was determined by ^{1}H NMR spectroscopy by integrating the CH_3 protons from the amine ligand backbone against an internal standard (ferrocene, 0.00336 M). Data are fit with nonlinear least-squares fitting to an equation describing exponential growth in [**21**]: [**21**] = $a + b(1 - e^{-k_{obs}t})$, R^2 = 0.99.

involves initial formation of a CO adduct with **2b**, followed by nucleophilic attack of PPh_3 on the terminal oxo.

Scheme 12

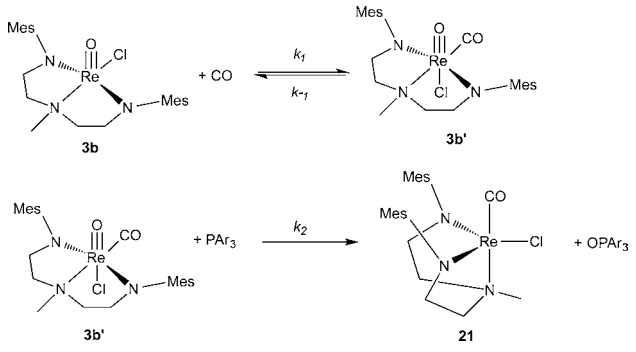

Kinetic experiments were also performed with a series of para-substituted aryl phosphines, PAr_3 (Ar = Ph, *p*-OMe-C_6H_4, *p*-CF_3-C_6H_4) to examine the effect on the observed rate constant, k_{obs}, of the Hammett substituent constant, σ. The Hammett plot obtained in this way resulted in a reaction constant ρ = −0.29 (see Supporting Information). As noted above, this value for the reaction constant is consistent with other oxorhenium complexes that exhibit electrophilic reactivity at the terminal oxo. This suggests that the oxygen atom transfer reaction is consistent with nucleophilic attack of phosphorus on an electrophilic metal oxo.

CONCLUSIONS

To summarize, a series of d^2 rhenium oxo complexes bearing the DAAm and DAP ligand frameworks have been shown to react with both Lewis acids (boron reagents) and Lewis bases (phosphine reagents). Traditionally, terminal oxo ligands in high-valent metal complexes are electrophilic, i.e., react with nucleophiles because of strong π bonding of the oxygen ligand lone pairs to empty metal d orbitals.[17] We have demonstrated that with the appropriate ligand set, these oxo ligands can react with both electrophiles and nucleophiles.[18]

EXPERIMENTAL SECTION

General Considerations. Complexes **1**−**7** were synthesized according to published procedures.[7e,l,9a−c] All reactions were conducted under dinitrogen in a Vacuum Atmosphere glovebox or using standard Schlenk line techniques unless otherwise noted. Solvents were degassed and purified with a solvent purification system (MBraun Inc.) and stored over 4 Å molecular sieves under dinitrogen atmosphere. All other reagents were purchased from commercial sources and used as received. ^{1}H, ^{13}C, ^{19}F, and ^{31}P NMR spectra were recorded on a Varian Mercury 400 MHz or a Varian Mercury 300 MHz spectrometer at room temperature. ^{1}H and ^{13}C NMR chemical shifts are listed in parts per million (ppm) and are referenced to residual protons or carbons of the deuterated solvents, respectively. ^{19}F NMR chemical shifts are referenced against an external standard (C_6F_6, −163 ppm). Elemental analyses were performed by Atlantic Microlabs, Inc. X-ray crystallography was performed at the X-ray Structural Facility of North Carolina State University by Dr. Paul Boyle.

General Synthesis of Rhenium Boron Adduct Complexes (8−16). The oxo−rhenium complex (0.155 mmol) was combined with 1.5 equiv of $B(C_6F_5)_3$ or $(Et_2O)BF_3$ in a small vial and dissolved in a minimal amount of dichloromethane. Slow diffusion of pentane into the solution yielded crystals of the rhenium boron adduct complex. The crystals were filtered and washed with excess pentane.

[DAAmRe(OB(C_6F_5)$_3$)CH_3] (aryl = C_6F_5), ***8.*** Isolated 149.7 mg, 82.1% yield. ^{1}H NMR (CD_2Cl_2, δ): 4.62 (m, 2H), 4.44 (s, 3H), 3.57 (m, 2H), 3.30 (s, 3H), 3.22 (m, 2H), 2.80 (m, 2H). ^{19}F NMR (CD_2Cl_2, δ): −134.78 (m, 15F), −149.95 (m, 2F), −150.30 (m, 2F), −158.50 (m, 2F), −163.33 (m, 2F), −163.55 (m, 2F). Anal. calcd for $C_{36}H_{14}BF_{25}N_3ORe$: C, 36,75; N, 3.75; H, 1.20. Found: C, 35.96; N, 3.53; H, 1.20.

[DAAmRe(OB(C_6F_5)$_3$)Cl] (aryl = C_6F_5), ***9.*** Isolated 95.3 mg, 56.5% yield. The complex is not air or solution stable, therefore only X-ray crystallographic characterization of the complex was obtained.

[DAPRe(OB(C_6F_5)$_3$)CH_3], ***10.*** Isolated 94.9 mg, 75% yield. ^{1}H NMR (CD_2Cl_2, δ): 8.30 (t, *J* 7.6 Hz, 1H, NC_2H_2CH) 7.92 (d, *J* 7.6 Hz, 2H, NC_2H_2CH) 6.88 (s, 2H, Mes-*meta*-H) 6.86 (s, 2H, Mes-*meta*-H) 6.12 (d, *J* 20.8 Hz, 2H, MesNHCH_2) 5.61 (d, *J* 20.8 Hz, 2H, MesNHCH_2) 3.46 (s, 3H, Re-CH_3) 2.26 (s, 6H, Mes-CH_3) 1.82 (s, 6H, Mes-CH_3) 1.30 (s, 6H, Mes-CH_3). ^{13}C NMR (CD_2Cl_2, δ): 167.02, 153.82, 143.21, 136.21, 134.42, 133.77, 129.85.19, 129.53, 117.32, 82.22, 37.77, 20.98, 18.13, 17.66. ^{19}F NMR (CD_2Cl_2, δ): −135.07 (m, 6F, phenyl-F), −159.93 (m, 3F, phenyl-*para*-F) −166.06 (m, 6F, phenyl-

dx.doi.org/10.1021/ja401390v | *J. Am. Chem. Soc.* 2013, 135, 9433−9441

F). Anal. calcd for $C_{44}H_{32}BF_{15}N_3ORe$: C, 48.01; N, 3.82; H, 2.93. Found: C, 47.61; N, 3.87; H, 3.04.

[DAPRe(OB(C_6F_5)$_3$)Cl], **11**. Isolated 117.2 mg, 85% yield. ^{1}H NMR (CD_2Cl_2, δ): 8.40 (t, *J* 7.2 Hz, 1H, NC_2H_2CH) 8.11 (d, *J* 7.2 Hz, 2H, NC_2H_2CH) 6.87 (s, 2H, Mes-*meta*-H) 6.82 (s, 2H, Mes-*meta*-H) 6.05 (d, *J* 20.8 Hz, 2H, MesNHCH_2) 5.70 (d, *J* 20.8 Hz, 2H, MesNHCH_2) 2.25 (s, 6H, Mes-CH_3) 1.90 (s, 6H, Mes-CH_3) 1.41 (s, 6H, Mes-CH_3). ^{13}C NMR (CD_2Cl_2, δ): 168.32, 157.00, 149. 35 (m, B(C_6F_5)$_3$), 146.97 (m B(C_6F_5)$_3$), 146.22, 141.61 (m, B(C_6F_5)$_3$), 139.00 (m, B(C_6F_5)$_3$), 138.60 (m, B(C_6F_5)$_3$), 136.61, 136.13 (m, B(C_6F_5)$_3$), 134.01, 133.48, 129.70, 129.30, 117.78, 84.55, 21.03, 18.71, 17.62. ^{19}F NMR (CD_2Cl_2, δ): −133.98 (m, 6F, phenyl-F), −158.72 (m, 3F, phenyl-*para*-F) −165.59 (m, 6F, phenyl-F). Anal. calcd for $C_{43}H_{29}BClF_{15}N_3ORe$: C, 46.05; N, 3.75; H, 2.61. Found: C, 46.19; N, 3.57; H, 2.79.

[DAPRe(OB(C_6F_5)$_3$)I], **12**. Isolated 103.8 mg, 80% yield. ^{1}H NMR (CD_2Cl_2, δ): 8.48 (t, *J* 7.8 Hz, 1H, NC_2H_2CH) 8.13 (d, *J* 7.8 Hz, 2H, NC_2H_2CH) 6.90 (s, 2H, Mes-*meta*-H) 6.88 (s, 2H, Mes-*meta*-H) 6.04 (d, *J* 21.0 Hz, 2H, MesNHCH_2) 5.64 (d, *J* 21.0 Hz, 2H, MesNHCH_2) 2.32 (s, 6H, Mes-CH_3) 1.93 (s, 6H, Mes-CH_3) 1.39 (s, 6H, Mes-CH_3). ^{19}F NMR (CD_2Cl_2, δ): −132.40 (m, 6F, phenyl-F), −159.92 (m, 3F, phenyl-*para*-F) −166.02 (m, 6F, phenyl-F). Anal. calcd for $C_{43}H_{29}BIF_{15}N_3ORe$: C: 42.59, N: 3.47, H: 2.41. Found: C, 41.91; N, 3.38; H, 2.50.

[DAAmRe(OB(C_6F_5)$_3$)(C(O)CH$_3$)] (aryl = C_6F_5), **13**. Isolated 96.3 mg, 76.3% yield. ^{1}H NMR (CD_2Cl_2, δ): 4.64 (m, 2H), 3.96 (m, 2H), 3.16 (s, 3H), 3.13 (m, 4H), 2.01 (s, 3H). The complex is not solution stable long enough to obtain a heteronuclear NMR spectrum. IR (KBr, thin film, $\nu_{C=O}$): 1649 cm^{-1}. Anal. calcd for $C_{37}H_{14}BF_{25}N_3O_2Re$: C, 36.89; N, 3.49; H, 1.17. Found: C, 36.24; N, 3.43; H, 1.08.

[DAPRe(OB(C_6F_5)$_3$)(C(O)CH$_3$)], **14**. Isolated 94.9 mg, 75% yield. The complex is not air or solution stable, therefore only X-ray crystallographic characterization of the complex was obtained.

[DAAmRe(O)(C(OBF$_3$)CH$_3$)] (aryl = C_6F_5), **15**. Isolated 65.2 mg, 57.9% yield. ^{1}H NMR (CD_2Cl_2, δ): 4.60 (m, 2H), 4.03 (m, 2H), 3.33 (s, 3H), 3.29 (m, 4H), 2.85 (s, 3H). ^{13}C NMR (CD_2Cl_2, δ): 299.4 (carbene C). ^{19}F NMR (CD_2Cl_2, δ): −147.09 (m, 2F), −149.00 (m, 3F), −152.46 (m, 2F), −160.89 (m, 2F), −164.94 (m, 4F). Anal. calcd for $C_{19}H_{14}BF_{13}N_3O_2Re$: C, 30.01; N, 5.53; H, 1.86. Found: C, 29.96; N, 5.50; H, 1.86.

[DAPRe(O)(C(OBF$_3$)CH$_3$)], **16**. Product was also washed with benzene. Isolated 80 mg, 95% yield. ^{1}H NMR (CD_3CN, δ): 8.31 (t, *J* 7.9 Hz, 1H, NC_2H_2CH) 7.81 (d, *J* 10.0 Hz, 2H, NC_2H_2CH) 6.86 (s, 2H, Mes-*meta*-H) 6.80 (s, 2H, Mes-*meta*-H) 5.86 (d, *J* 20.7 Hz, 2H, MesNCH_2) 5.48 (d, *J* 21.1 Hz, 2H, MesNCH_2) 2.65 (s, 3H, carbene-CH_3) 2.50 (s, 6H, Mes-CH_3) 2.27 (s, 6H, Mes-CH_3) 1.91 (s, 6H, Mes-CH_3). ^{13}C NMR (CD_3CN, δ): 299.0, 166.61, 153.58, 144.17, 136.10, 136.04, 135.63, 129.92, 129.46, 119.78, 74.71, 42.00, 20.92, 18.40, and 18.10 Anal. calcd for $C_{30}H_{35}BF_3N_3O_2Re$ (with 0.5 C_6H_6): C, 49.79; N, 5.81; H, 4.88. Found: C, 49.39; N, 5.38; H, 4.68.

[DAAmRe(CO)Cl] (aryl = Mes), **21**. To a 50 mL stainless steel glass-lined Parr reactor, **3b** (100.1 mg, 0.170 mmol) and triphenylphosphine (89.1 mg, 0.320 mmol) were added and dissolved in 1,2-dichloroethane (∼20 mL). The reactor was purged and pressurized with CO (800 psi), and the solution was stirred at 80 °C for 3 days. The solvent was removed under reduced pressure. The resulting orange oil was dissolved in a minimal amount of dichloromethane, precipitated with excess pentane, and filtered to yield an orange powder. Crystals of **21** were obtained by the slow diffusion of pentane into a concentrated dichloromethane solution of the orange powder (25.4 mg, 24.9% yield). ^{1}H NMR (CD_2Cl_2, δ): 6.88 (s, 2H), 6.85 (s, 2H), 3.78 (m, 4H), 3.04 (m, 4H), 2.96 (s, 3H), 2.30 (s, 6H), 2.17 (s, 6H), 2.11 (s, 6H). ^{13}C NMR (CD_2Cl_2, δ): 196.0, 158.4, 135.5, 133.0, 130.3, 129.2, 129.1, 63.2, 59.0, 45.3, 20.9, 19.7, 19.5. IR (KBr, thin film, $\nu_{C\equiv O}$): 1860 cm^{-1}. Anal. calcd for $C_{24}H_{33}ClN_3ORe$: C, 47.95; N, 6.99; H, 5.53. Found: C, 48.76; N, 6.89; H, 5.54.

General Procedure for Kinetic Experiments. For each set of reactions, in nine 5 mL glass storage tubes, **3** (5.0 mg, 0.0084 mmol) was combined with *X* equiv (*X* = 10, 20 or 30) of the respective phosphine in 0.6 mL CD_3CN. The storage tube was pressurized with *X* psi (*X* = 30, 45, or 60) of CO after the storage tube was subjected to two freeze−pump−thaw cycles. The reaction mixture was heated at 80 °C. Each reaction was stopped at a different time point in order to obtain the reaction profile. The [**21**] was determined by ^{1}H NMR spectroscopy by integrating the CH_3 protons from the amine ligand backbone against an internal standard (ferrocene, 0.00336 M).

Computational Methods. Theoretical calculations have been carried out using the Gaussian09[16] implementation of B3PW91 (the B3 exchange functional[13] and PW91 correlation functional)[19] DFT.[12] All geometry optimizations were carried out using tight convergence criteria ("opt = tight") and pruned ultrafine grids ("Int = ultrafine"). All calculations were conducted with the same basis set combination. The basis set for rhenium was the small-core (311111,22111,411) → [6s5p3d] Stuttgart−Dresden basis set and relativistic effective core potential (RECP) combination (SDD)[20] with an additional *f* polarization function.[21] The 6-31G(d,p) basis sets were used for all other atoms. Cartesian *d* functions were used throughout, i.e., there are six angular basis functions per *d* function. All structures were fully optimized, and analytical frequency calculations were performed on all structures to ensure either a zeroth-order saddle point (a local minimum) or a first-order saddle point (transition state: TS) was achieved. The minima associated with each transition state was determined by animation of the imaginary frequency and, if necessary, with intrinsic reaction coordinate (IRC) calculations. Solvation energies were computed geometries optimized in the gas phase using the SMD method,[22] with benzene as the solvent, as implemented in Gaussian 09. In this method an IEFPCM calculation is performed with radii and electrostatic terms from Truhlar and co-workers' SMD solvation model.[15] In this manuscript energies are reported in kcal/mol with gas-phase energies in parentheses and solvation energies without parentheses.

■ ASSOCIATED CONTENT

Ⓢ Supporting Information

Cartesian coordinates for all optimized complexes as well as the full Gaussian 09 reference. Experimental data and tables for X-ray data. Details of kinetic experiments, kinetic plots, and rate law derivation for mechanism in Scheme 12. This material is available free of charge via the Internet at http://pubs.acs.org.

■ AUTHOR INFORMATION

Corresponding Author

eaison@ncsu.edu

Author Contributions

†J.L.S. and C.P.L. contributed equally.

Notes

The authors declare no competing financial interest.

■ ACKNOWLEDGMENTS

We acknowledge North Carolina State University and the National Science Foundation via the CAREER Award (CHE-0955636) for funding.

■ REFERENCES

(1) (a) Bukowski, M. R.; Koehntop, K. D.; Stubna, A.; Bominaar, E. L.; Halfen, J. A.; Muenck, E.; Nam, W.; Que, L., Jr. *Science* **2005**, *310*, 1000−1002. (b) England, J.; Guo, Y.; Van, H. K. M.; Cranswick, M. A.; Rohde, G. T.; Bominaar, E. L.; Munck, E.; Que, L. *J. Am. Chem. Soc.* **2011**, *133*, 11880−11883. (c) England, J.; Martinho, M.; Farquhar, E. R.; Frisch, J. R.; Bominaar, E. L.; Munck, E.; Que, L., Jr. *Angew. Chem., Int. Ed.* **2009**, *48*, 3622−3626. (d) Gupta, R.; Borovik, A. S. *J. Am. Chem. Soc.* **2003**, *125*, 13234−13242. (e) Krebs, C.; Fujimori, D. G.; Walsh, C. T.; Bollinger, J. M., Jr. *Acc. Chem. Res.* **2007**, *40*, 484−492. (f) Nam, W. *Acc. Chem. Res.* **2007**, *40*, 522−531. (g) Que, L. *Acc. Chem. Res.* **2007**, *40*, 493−500. (h) van, E. R. *Chem. Rev.* **2005**, *105*, 1917−1921.

(2) (a) Arzoumanian, H. *Coord. Chem. Rev.* **1998**, *178*−*180*, 191−202. (b) Brondino, C. D.; Rivas, M. G.; Romao, M. J.; Moura, J. J. G.; Moura, I. *Acc. Chem. Res.* **2006**, *39*, 788−796. (c) Donahue, J. P.; Lorber, C.; Nordlander, E.; Holm, R. H. *J. Am. Chem. Soc.* **1998**, *120*, 3259−3260. (d) Harlan, E. W.; Berg, J. M.; Holm, R. H. *J. Am. Chem. Soc.* **1986**, *108*, 6992−7000. (e) Heinze, K.; Fischer, A. *Eur. J. Inorg. Chem.* **2010**, 1939−1947. (f) Hoffman, J. T.; Einwaechter, S.; Chohan, B. S.; Basu, P.; Carrano, C. J. *Inorg. Chem.* **2004**, *43*, 7573−7575. (g) Holm, R. H. *Coord. Chem. Rev.* **1990**, *100*, 183−221. (h) Holm, R. H.; Solomon, E. I.; Majumdar, A.; Tenderholt, A. *Coord. Chem. Rev.* **2011**, *255*, 993−1015. (i) Lee, S. C.; Holm, R. H. *Inorg. Chim. Acta* **2008**, *361*, 1166−1176. (j) Lim, B. S.; Holm, R. H. *J. Am. Chem. Soc.* **2001**, *123*, 1920−1930. (k) McMaster, J.; Tunney, J. M.; Garner, C. D. *Prog. Inorg. Chem.* **2003**, *52*, 539−583. (l) McNamara, J. P.; Joule, J. A.; Hillier, I. H.; Garner, C. D. *Chem. Commun.* **2005**, 177−179. (m) Moura, J. J. G.; Brondino, C. D.; Trincao, J.; Romao, M. J. *J. Biol. Inorg. Chem.* **2004**, *9*, 791−799. (n) Peariso, K.; McNaughton, R. L.; Kirk, M. L. *J. Am. Chem. Soc.* **2002**, *124*, 9006−9007. (o) Pushie, M. J.; George, G. N. *Coord. Chem. Rev.* **2011**, *255*, 1055−1084. (p) Schultz, B. E.; Gheller, S. F.; Muetterties, M. C.; Scott, M. J.; Holm, R. H. *J. Am. Chem. Soc.* **1993**, *115*, 2714−22. (q) Smith, P. D.; Millar, A. J.; Young, C. G.; Ghosh, A.; Basu, P. *J. Am. Chem. Soc.* **2000**, *122*, 9298−9299. (r) Sugimoto, H.; Tarumizu, M.; Tanaka, K.; Miyake, H.; Tsukube, H. *Dalton Trans.* **2005**, 3558−3565. (s) Wallace, D.; Gibson, L. T.; Reglinski, J.; Spicer, M. D. *Inorg. Chem.* **2007**, *46*, 3804−3806. (t) Wang, J.-J.; Tessier, C.; Holm, R. H. *Inorg. Chem.* **2006**, *45*, 2979−2988.

(3) (a) Barber, J. *Inorg. Chem.* **2008**, *47*, 1700−1710. (b) Guskov, A.; Gabdulkhakov, A.; Broser, M.; Gloeckner, C.; Hellmich, J.; Kern, J.; Frank, J.; Mueh, F.; Saenger, W.; Zouni, A. *ChemPhysChem* **2010**, *11*, 1160−1171. (c) Lee, C.-I.; Brudvig, G. W. *J. Chin. Chem. Soc.* **2004**, *51*, 1221−1228. (d) Siegbahn, P. E. M. *Acc. Chem. Res.* **2009**, *42*, 1871−1880. (e) Park, Y. J.; Ziller, J. W.; Borovik, A. S. *J. Am. Chem. Soc.* **2011**, *133*, 9258−9261. (f) Taguchi, T.; Gupta, R.; Lassalle-Kaiser, B.; Boyce, D. W.; Yachandra, V. K.; Tolman, W. B.; Yano, J.; Hendrich, M. P.; Borovik, A. S. *J. Am. Chem. Soc.* **2012**, *134*, 1996−1999. (g) Kanady, J. S.; Mendoza-Cortes, J. L.; Tsui, E. Y.; Nielsen, R. J.; Goddard, W. A.; Agapie, T. *J. Am. Chem. Soc.* **2012**, *135* (3), 1073−1082. (h) Kanady, J. S.; Tsui, E. Y.; Day, M. W.; Agapie, T. *Science* **2011**, *333*, 733−736.

(4) (a) Chronister, C. W.; Binstead, R. A.; Ni, J.; Meyer, T. J. *Inorg. Chem.* **1997**, *36*, 3814−3815. (b) Concepcion, J. J.; Jurss, J. W.; Brennaman, M. K.; Hoertz, P. G.; Patrocinio, A. O. T.; Murakami, I. N. Y.; Templeton, J. L.; Meyer, T. J. *Acc. Chem. Res.* **2009**, *42*, 1954−1965. (c) Concepcion, J. J.; Jurss, J. W.; Templeton, J. L.; Meyer, T. J. *Proc. Natl. Acad. Sci. U.S.A.* **2008**, *105*, 17632−17635. (d) Gagliardi, C. J.; Vannucci, A. K.; Concepcion, J. J.; Chen, Z.; Meyer, T. J. *Energy Environ. Sci.* **2012**, *5*, 7704−7717. (e) Jurss, J. W.; Concepcion, J. J.; Butler, J. M.; Omberg, K. M.; Baraldo, L. M.; Thompson, D. G.; Lebeau, E. L.; Hornstein, B.; Schoonover, J. R.; Jude, H.; Thompson, J. D.; Dattelbaum, D. M.; Rocha, R. C.; Templeton, J. L.; Meyer, T. J. *Inorg. Chem.* **2012**, *51*, 1345−1358. (f) Kuznetsov, A. E.; Geletii, Y. V.; Hill, C. L.; Morokuma, K.; Musaev, D. G. *J. Am. Chem. Soc.* **2009**, *131*, 6844−6854. (g) Li, X.; Chen, G.; Schinzel, S.; Siegbahn, P. E. M. *Dalton Trans.* **2011**, *40*, 11296−11307. (h) Limburg, B.; Bouwman, E.; Bonnet, S. *Coord. Chem. Rev.* **2012**, *256*, 1451−1467. (i) Liu, F.; Concepcion, J. J.; Jurss, J. W.; Cardolaccia, T.; Templeton, J. L.; Meyer, T. J. *Inorg Chem* **2008**, *47*, 1727−52. (j) Moonshiram, D.; Jurss, J. W.; Concepcion, J. J.; Zakharova, T.; Alperovich, I.; Meyer, T. J.; Pushkar, Y. *J. Am. Chem. Soc.* **2012**, *134*, 4625−4636. (k) Stull, J. A.; Britt, R. D.; McHale, J. L.; Knorr, F. J.; Lymar, S. V.; Hurst, J. K. *J. Am. Chem. Soc.* **2012**, *134*, 19973−19976.

(5) Winkler, J. R.; Gray, H. B. *Struct. Bonding (Berlin)* **2012**, *142*, 17−28.

(6) Palucki, M.; Finney, N. S.; Pospisil, P. J.; Gueler, M. L.; Ishida, T.; Jacobsen, E. N. *J. Am. Chem. Soc.* **1998**, *120*, 948−954.

(7) (a) Basu, P.; Kail, B. W.; Young, C. G. *Inorg. Chem.* **2010**, *49*, 4895−4900. (b) Cai, Y.; Ellern, A.; Espenson, J. H. *Inorg. Chem.* **2005**, *44*, 2560−2565. (c) Conry, R. R.; Mayer, J. M. *Inorg. Chem.* **1990**, *29*, 4862−7. (d) Espenson, J. H. *Coord. Chem. Rev.* **2005**, *249*, 329−341. (e) Ison, E. A.; Cessarich, J. E.; Travia, N. E.; Fanwick, P. E.; Abu-Omar, M. M. *J. Am. Chem. Soc.* **2007**, *129*, 1167−1178. (f) Koshino, N.; Espenson, J. H. *Inorg. Chem.* **2003**, *42*, 5735−5742. (g) Over, D. E.; Critchlow, S. C.; Mayer, J. M. *Inorg. Chem.* **1992**, *31*, 4643−8. (h) Reynolds, M. S.; Berg, J. M.; Holm, R. H. *Inorg. Chem.* **1984**, *23*, 3057−62. (i) Seymore, S. B.; Brown, S. N. *Inorg. Chem.* **2000**, *39*, 325−332. (j) Wang, Y.; Espenson, J. H. *Inorg. Chem.* **2002**, *41*, 2266−2274. (k) Wang, Y.; Espenson, J. H. *Inorg Chem* **2002**, *41*, 2266−74. (l) Feng, Y.; Aponte, J.; Houseworth, P. J.; Boyle, P. D.; Ison, E. A. *Inorg. Chem.* **2009**, *48*, 11058−11066.

(8) (a) Betley, T. A.; Surendranath, Y.; Childress, M. V.; Alliger, G. E.; Fu, R.; Cummins, C. C.; Nocera, D. G. *Philos. Trans. R. Soc., B* **2008**, *363*, 1293−303. (b) Betley, T. A.; Wu, Q.; Van, V. T.; Nocera, D. G. *Inorg. Chem.* **2008**, *47*, 1849−1861.

(9) (a) Lilly, C. P.; Boyle, P. D.; Ison, E. A. *Dalton Trans.* **2011**, *40*, 11815−11821. (b) Lilly, C. P.; Boyle, P. D.; Ison, E. A. *Organometallics* **2012**, *31*, 4295−4301. (c) Smeltz, J. L.; Boyle, P. D.; Ison, E. A. *J. Am. Chem. Soc.* **2011**, *133*, 13288−13291. (d) Smeltz, J. L.; Boyle, P. D.; Ison, E. A. *Organometallics* **2012**, *31*, 5994−5997. (e) Smeltz, J. L.; Webster, C. E.; Ison, E. A. *Organometallics* **2012**, *31*, 4055−4062.

(10) (a) Peryshkov, D. V.; Schrock, R. R.; Takase, M. K.; Muller, P.; Hoveyda, A. H. *J. Am. Chem. Soc.* **2011**, *133*, 20754−20757. (b) Sanchez-Nieves, J.; Frutos, L. M.; Royo, P.; Castano, O.; Herdtweck, E. *Organometallics* **2005**, *24*, 2004−2007. (c) Sanchez-Nieves, J.; Frutos, L. M.; Royo, P.; Castano, O.; Herdtweck, E.; Mosquera, M. E. G. *Inorg. Chem.* **2010**, *49*, 10642−10648. (d) Sanchez-Nieves, J.; Royo, P.; Mosquera, M. E. G. *Eur. J. Inorg. Chem.* **2006**, 127−132. (e) Barrado, G.; Doerrer, L.; Green, M. L. H.; Leech, M. A. *J. Chem. Soc., Dalton Trans.* **1999**, 1061−1066. (f) Doerrer, L. H.; Galsworthy, J. R.; Green, M. L. H.; Leech, M. A. *J. Chem. Soc., Dalton Trans.* **1998**, 2483−2488. (g) Doerrer, L. H.; Galsworthy, J. R.; Green, M. L. H.; Leech, M. A.; Muller, M. *J. Chem. Soc., Dalton Trans.* **1998**, 3191−3194. (h) Fischer, J.; Kress, J.; Osborn, J. A.; Ricard, L.; Wesolek, M. *Polyhedron* **1987**, *6*, 1839−42. (i) Galsworthy, J. R.; Green, J. C.; Green, M. L. H.; Muller, M. *J. Chem. Soc., Dalton Trans.* **1998**, 15−20. (j) Galsworthy, J. R.; Green, M. L. H.; Muller, M.; Prout, K. *J. Chem. Soc., Dalton Trans.* **1997**, 1309−1313.

(11) (a) Smeltz, J. L.; Boyle, P. D.; Ison, E. A. *J. Am. Chem. Soc.* **2011**, *133*, 13288−13291. (b) Smeltz, J. L.; Webster, C. E.; Ison, E. A. *Organometallics* **2012**, *31*, 4055−4062.

(12) Parr, R. G., Yang, W. *Density Functional Theory of Atoms and Molecules*; Oxford University Press: New York, 1989.

(13) Becke, A. D. *J. Chem. Phys.* **1993**, *98*, 5648−52.

(14) Ehlers, A. W.; Boehme, M.; Dapprich, S.; Gobbi, A.; Hoellwarth, A.; Jonas, V.; Koehler, K. F.; Stegmann, R.; Veldkamp, A.; et al. *Chem. Phys. Lett.* **1993**, *208*, 111−14.

(15) Tomasi, J.; Mennucci, B.; Cammi, R. *Chem. Rev.* **2005**, *105*, 2999−3093.

(16) Frisch, M. J.; Trucks, G. W.; Schlegel, H. B.; et al. *Gaussian 09*, revisions, A.02; Gaussian, Inc.: Wallingford, CT, 2009.

(17) For an example of a d^4 oxo, see: Fukuzumi, S.; Morimoto, Y.; Kotani, H.; Naumov, P.; Lee, Y.-M.; Nam, W. *Nat. Chem.* **2010**, *2*, 756−759.

(18) For an example of ambiphilic metal nitrides, see: (a) Crevier, T. J.; Bennett, B. K.; Soper, J. D.; Bowman, J. A.; Dehestani, A.; Hrovat, D. A.; Lovell, S.; Kaminsky, W.; Mayer, J. M. *J. Am. Chem. Soc.* **2001**, *123*, 1059−1071. (b) J. Crevier, T.; Lovell, S.; M. Mayer, J. *Chem. Commun.* **1998**, *0*, 2371−2372.

(19) Perdew, J. P.; Chevary, J. A.; Vosko, S. H.; Jackson, K. A.; Pederson, M. R.; Singh, D. J.; Fiolhais, C. *Phys. Rev. B: Condens. Matter* **1992**, *46*, 6671−87.

(20) Dolg, M.; Stoll, H.; Preuss, H.; Pitzer, R. M. *J. Phys. Chem.* **1993**, *97*, 5852−9.

(21) Hehre, W. J.; Ditchfield, R.; Pople, J. A. *J. Chem. Phys.* **1972**, *56*, 2257−61.

(22) Marenich, A. V.; Cramer, C. J.; Truhlar, D. G. *J. Phys. Chem. B* **2009**, *113*, 6378−6396.